Supporting Information: The role of interface in stabilizing reaction intermediates for hydrogen evolution in aprotic electrolyte.

Ivano E. Castelli,[1,2,*] Milena Zorko,[3] Thomas M. Østergaard,[1] Pedro Martins,[3] Pietro P. Lopes,[3] Byron K. Antonopoulos,[4] Filippo Maglia,[4,5] Nenad M. Markovic,[3] Dusan Strmcnik,[3,*] and Jan Rossmeisl[1,*]

[1]Nano-Science Center, Department of Chemistry, University of Copenhagen, DK-2100, Copenhagen Ø, Denmark
[2]Department of Energy Conversion and Storage, Technical University of Denmark, DK-2800, Kgs. Lyngby, Denmark
[3]Materials Science Division, Argonne National Laboratory, Argonne, IL, USA
[4]Battery Cell Technology, BMW Group, München, Germany
[5]Institute for Advanced Study, Technical University of Munich, Lichtenbergstrasse 2a, D-85748 Garching, Germany
[*]e-mail: ivca@dtu.dk (IEC); strmcnik@anl.gov (DS); jan.rossmeisl@chem.ku.dk (JR)

Computational Methods

In this work, we have used two different computational methodologies based on Density Functional Theory (DFT) depending on the purpose of the calculations: standard DFT has been used to calculate the descriptors for the electrochemical response and the reaction paths, while ab-initio molecular dynamics (AIMD) has been used to calculate the solid/liquid interface and the phase diagrams of Li in the electrolyte. In this section, we report the computational details for the two methodologies.

All calculations have been performed using the GPAW code [1,2] combined with the ASE package for handling the crystal structures.[3] These calculations are collected in a ASE database format available online in the KatlaDB repository. [https://nano.ku.dk/english/research/theoretical-electrocatalysis/katladb/]

At first, we have performed standard DFT to investigate the descriptors for the electrochemical response. Even if it does not give accurate results for the electrode/electrolyte interface, this method gives valuable information that can be later on verified using AIMD. The calculations for these descriptors (Figure S3) are performed using a 4x4x4 unit cells with the two bottom layers kept frozen to reproduce the bulk of the slab and the two top layer let free to relax as well as the adsorbate. We include a vacuum of 16Å to separate the periodic images in the direction normal to the surface and we apply a dipole correction to separate the contribution to the electrostatic interaction between the periodic images. We use a $4 \times 3 \times 1$ Monkhorst-Pack k-point grid, 0.2 grid spacing, and BEEF-vdW as exchange-correlation functional.[4] The adsorption energy, ΔE, is calculated as the difference in the DFT total energy between the surface with and without the adsorbate ($E_{slab+ads}$ and E_{slab}, respectively) minus the adsorbate in its standard state (E_{ads}):

$$\Delta E = E_{slab+ads} - E_{slab} - E_{ads}$$

As standard states for the adsorbates, we use the metal bulk reference for all the species, except for hydrogen and fluorine, for which we use H_2 and F_2 molecules, respectively.

After this preliminary investigation, we have explicitly included the electrolyte in our calculations. To investigate the structure of the interface (Figure 1b and S3), we have used ab-initio molecular dynamics (AIMD) simulations in which each step of a molecular dynamic simulation, run at room temperature, is

calculated at the DFT level.[5] All the calculations are performed in the Linear Combination of Atomic Orbitals (LCAO) mode,[6] using double zeta polarized basis set, RPBE as exchange-correlation functional,[7] a single K-point (gamma), and we apply the dipole correction to the electrostatic potential in the direction normal to the surface. A Berendsen thermostat,[8] with characteristic time of 2000 fs and a time step of 1 fs, has been used to control the temperature in the molecular dynamics. To obtain the phase diagrams of Li in the electrolyte, we have to consider different initial structures, namely different possible positions and coverages of Li. In each structure, we can distinguish three regions: (i) a fixed metal slab composed of 4x4x4 unit cells, (ii) the electrolyte, and (iii) a fixed top layer of the electrolyte, as shown in the inset of Figure 1b. As fixed top layer, we use the ice structure of ethylene carbonate (EC),[9,10] with total dipole along the direction normal to the surface equal zero. The top layer has the double function of confining the electrolyte at the correct experimental density and mimicking the electrolyte bulk structure. In addition, to not affect the orientation of the molecules, the dipole in the normal direction should be zero. LP57 is composed of ethylene carbonate (EC) and ethyl methyl carbonate (EMC) with a ratio 3:7 in weight. This corresponds, in our simulations, to 8 molecules of EMC and 4 of EC. An example of the used structure is shown in the inset of Figure 1a. Each composition of the electrolyte has been thermalized until the total energies oscillates in a range of no more than ±50 meV/atom, which is typically achieved within 2 ps of the AIMD simulations. Afterwards, each trajectory used to estimate the phase diagram is at least 2 ps long. The distribution of the work functions normal to the surface for each trajectory shows a Gaussian shape, which indicates that the dipole is uncorrelated from the initial structure and the sampling is long enough. This would not be enough if we were interested in the structure of the electrolyte and longer trajectories would be needed. On the other side, the purpose of the molecular dynamics here is to generate a sample of electrolyte structure that allows to control the electrochemical potential at the surface and this can be achieved with trajectories relatively short. Longer trajectories would not improve our results. The energy difference between the structures is calculated using an equivalent for Li of the generalized computational hydrogen electrode for Li. The Gibbs free energy, G, is calculated as a function of the enthalpy of the system, ΔE, and of the electronic work function (the calculated work function), U_e, with respect to the Li/Li$^+$ potential, Φ: $G = \Delta E - n_{Li}(\Phi - U_e)$, where n_{Li} is the number of Li atoms in the configuration. In addition, we perform a grand canonical Metropolis Monte Carlo algorithm at 300 K before calculating the phase diagram. The purpose of the MC algorithm is to walk around all the sampled states and the trial state can add or remove up to 3 Li atoms (adsorbed or solvated) to the accepted state with equal probability. From the MC simulations, we obtain the minimum energy configuration as a function of the work function and thus the phase diagram of Li in LP57. It is important to note that the work function range is divided into bins and the ground state configuration is identified for each bin. If the binning is too dense, a longer sampling is needed to converge the averages in each bin. More details about the methodology can be found in the literature.[5] A similar procedure has been previously applied to study water, electrochemical CO reduction, and the LP57. [5,11–13]

Accurate calculations have been performed on top of the various solid/liquid structures at different electrostatic potential and Li coverage obtained from the AIMD simulations. In particular, for the descriptors shown in Figure 1c, we start from the structure of the electrolyte at a potential corresponding to the adsorption potential of Li, indicated with an arrow in Figure 1b. The adsorption energy ΔE_{Li} is now calculated including the electrolyte, as:

$$\Delta E_{Li} = E_{slab+electrolyte+ads} - E_{slab+electrolyte} - E_{ads}$$

These calculations have been performed in the grid mode, using RPBE, and a denser k-point grid of 2x2x1. Similar approach has been used to calculate the reaction paths shown in Figure 1d and 2a. For these calculations, the energy difference between the relevant structures is calculated simply as the difference between the total energies since all structures have the same number of atoms, just in different configurations.

Experimental Methods

Extended surface electrode preparation: Pt(111), Ir(111), Au(111), Au (110), Au (100) and Cu (111) electrodes were prepared by inductive heating for 5 min at 1,050 °C for Pt, 800 °C for Au and Cu and 1,200 °C for Ir electrodes in an argon hydrogen flow (3% hydrogen). The annealed specimens were cooled slowly to room temperature under an inert atmosphere and then assembled into a rotating disk electrode (RDE). Voltammograms were recorded in argon-saturated electrolytes.

Chemicals: For non-aqueous experiments involving HF electroreduction, LP57 (1M $LiPF_6$ in EC:EMC (3:7 wt)) purchased from BASF, was used. The HF content measured in LP57 was 30 ppm. Argon gas used for purging was 5N5 quality and purchased from Airgas. In experiments involving H_2O and methanesulfonic acid (MSA) as proton donors, 1M $LiClO_4$ (Sigma Aldrich) in EC:EMC (3:7 wt) was used. H_2O and MSA (both purchased from Sigma Aldrich) were added just before the experiment.

Electrochemical measurements: A three-electrode glass cell was used in all experiments. All of the experiments executed in this cell were performed within minutes of introducing the electrolyte into the cell. Gold wire was used as a counter electrode and Ag/AgCl or Ag/Ag^+ electrode was used as reference electrodes for aqueous and non-aqueous experiments, respectively. All potentials are given on Li/Li^+ scale. The conversion of Ag/Ag^+ to Li/Li^+ scale was done by electrodepositing and stripping Li on a glassy carbon electrode in a separate experiment, establishing the position of the Li/Li^+ reversible potential. Experiments were controlled using an Autolab PGSTAT 302N potentiostat. For the rotating disk experiments, a Pine MSR electrode rotator was used. All reported voltammograms were first cycle measurements (unless explicitly stated otherwise) to limit the effects of possible contamination from the electrolyte. All non-aqueous electrochemical experiments were performed inside the glovebox.

Voltammetry

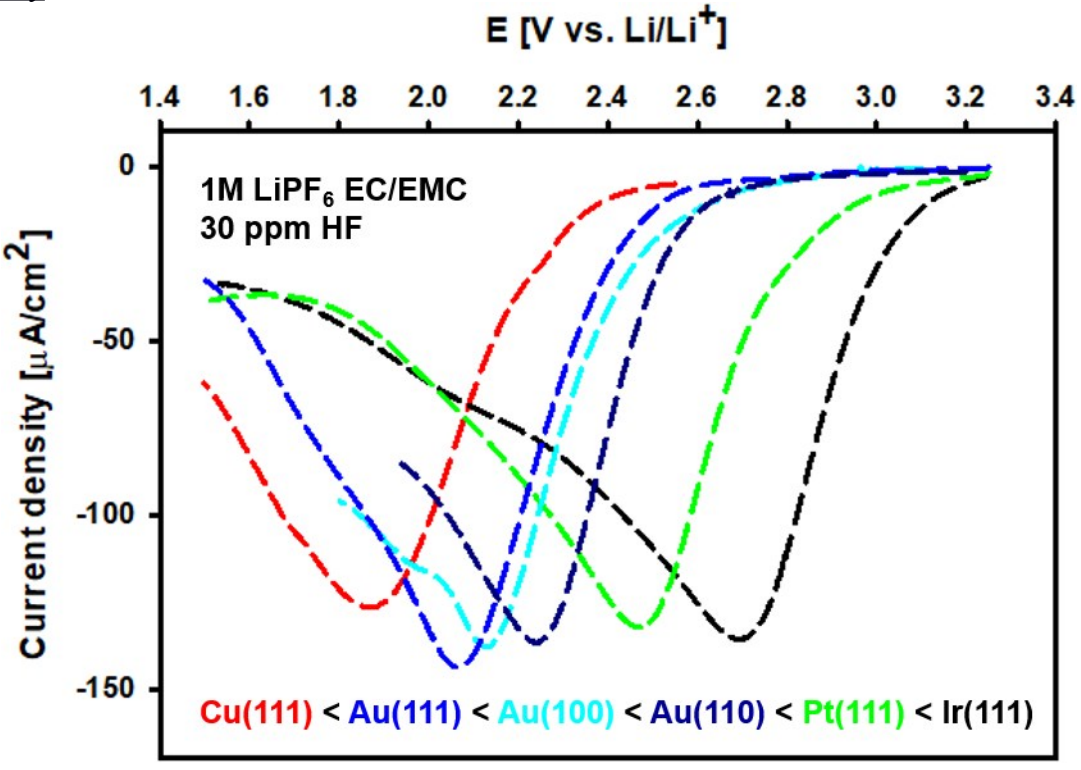

Figure S1: Measured voltammograms for LiPF6 in Cu(111), Au(111,100, and 110), Pt(111), and Ir(111) under stagnant conditions.

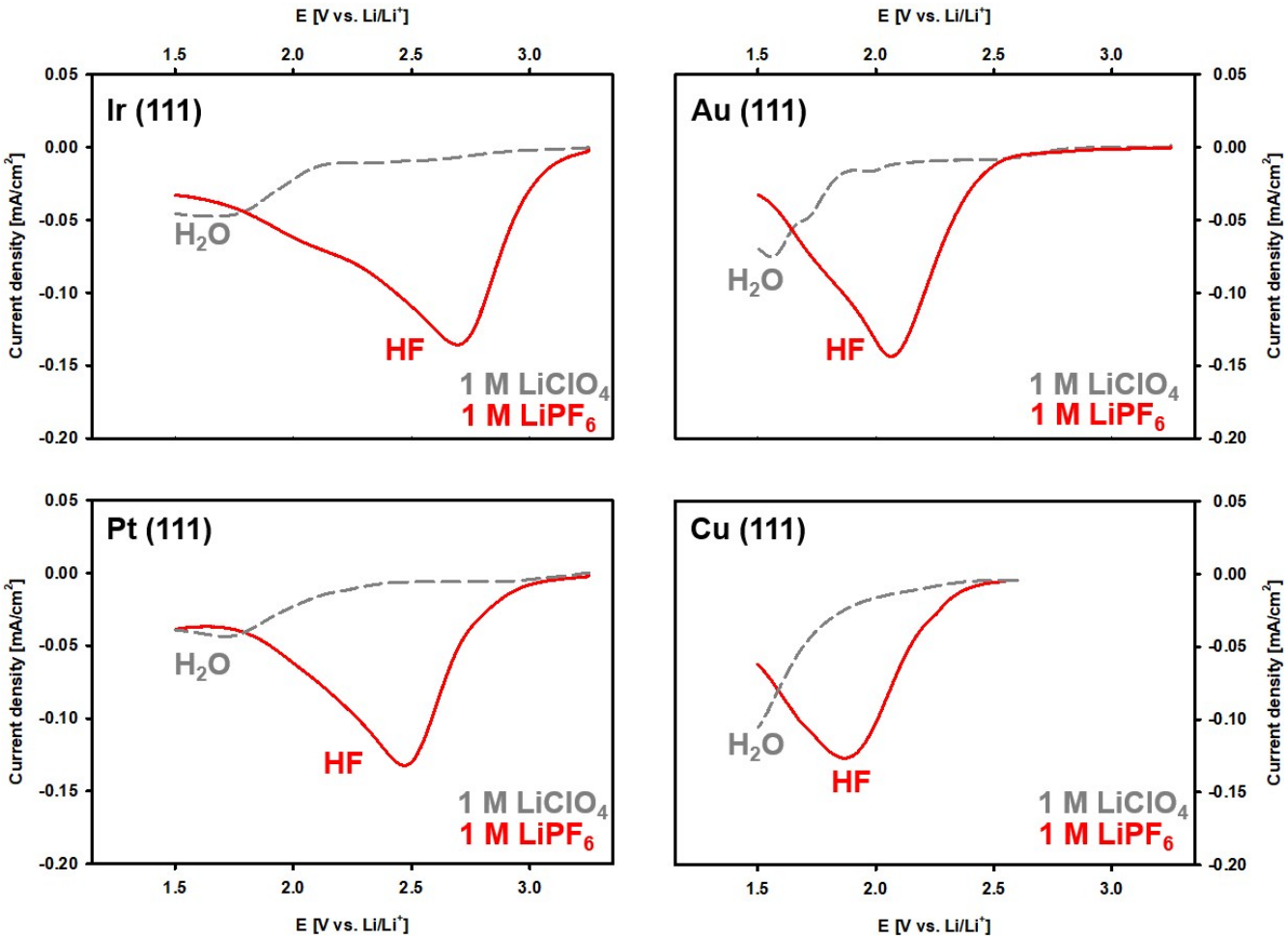

Figure S2: Comparison between the measured voltammograms in 1 M$LiPF_6$ and 1 M $LiClO_4$ in EC/EMC for the 4 metal surfaces considered in this work. The results in $LiClO_4$ electrolyte (with no added water) show the electrochemical responses in the absence of HF. The observed currents below 2 V are mainly due to the reduction of trace amounts of water, which are inherently present in the $LiClO_4$ electrolyte.

Descriptors for the Electrochemical Response in Vacuum

Because of the high computational cost of AIMD, the possible descriptors for the electrochemical response have been first investigated considering only the metal slab and adsorbate without electrolyte (Figure S1). The adsorption energy of H, Li, F, and HF is considered as possible descriptor for the measured first electrochemical response. Only the adsorption of Li correlates with the measured electrochemical response. This indicates that the presence of Li at the interface plays a key role in the electrochemical reactions. This correlation is valid not only for (111) terminations, but also for (100) and Au(110) surfaces. Due to the high computational cost, AIMD have not been run for these two terminations, but similar results as for (111) surfaces are expected.

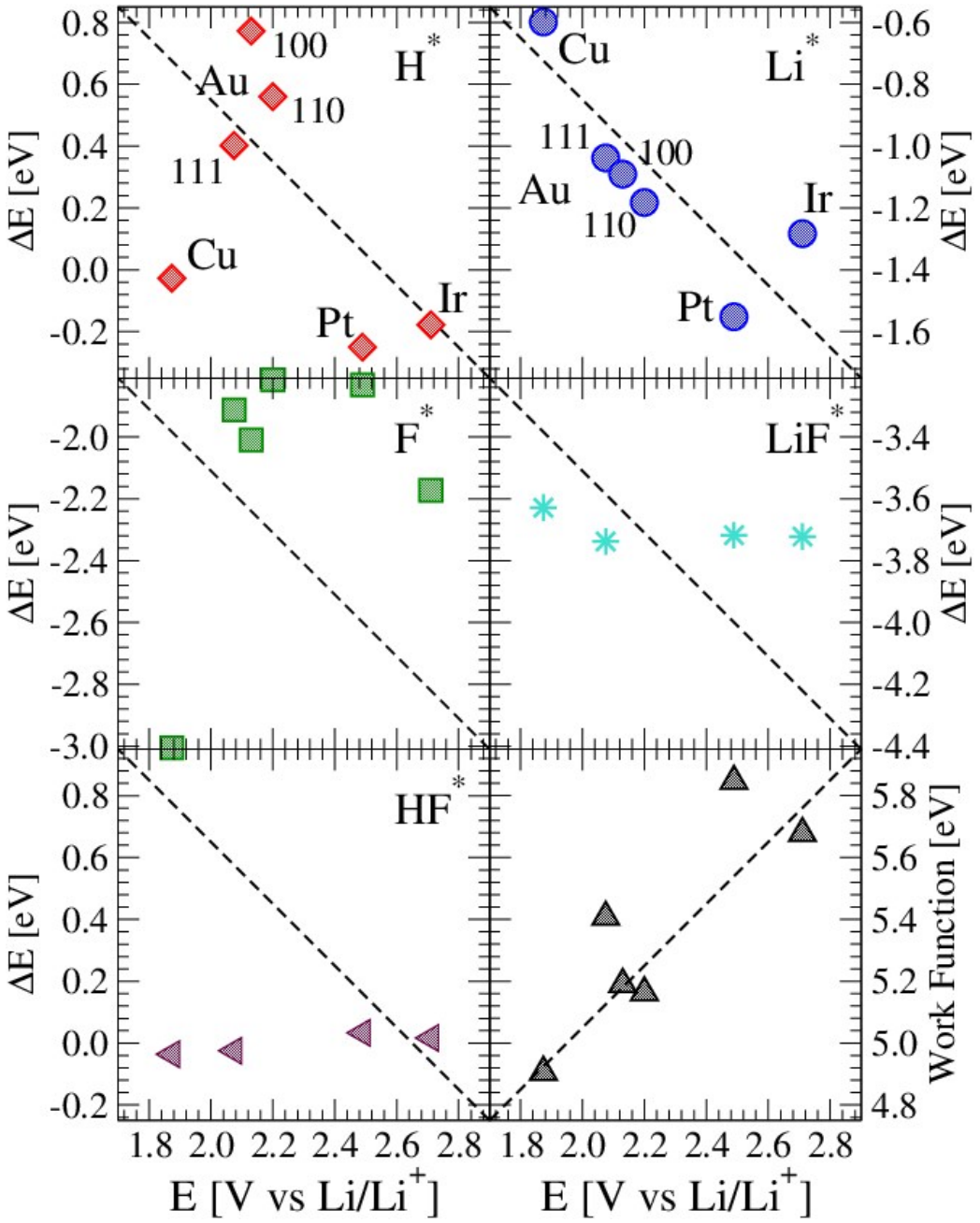

Figure S3: descriptors for the first electrochemical response in vacuum. The possible descriptors investigated here are the adsorption energy of H, Li, F, LiF, and HF as well as the work function of the clean slab.

Phase diagram of EC:EMC on different metals

AIMD simulations have been performed for all the surfaces investigated here. The main effect of the surface is on the adsorption potential of Li, which shifts following a change in the work function as shown in Figure 1c.2. The phase diagrams are shown in Figure S4.

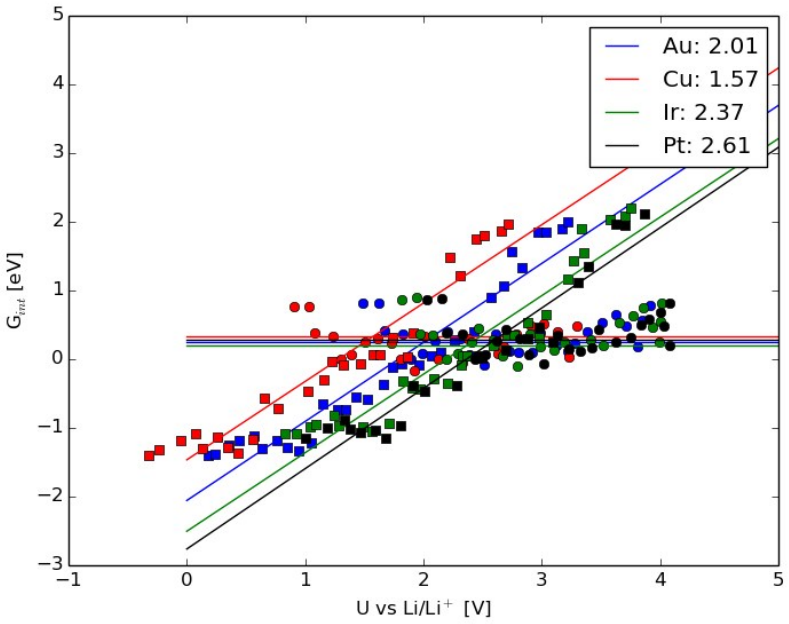

Figure S4: phase diagrams on the different metals. The adsorption potential of Li is indicated in the legend.

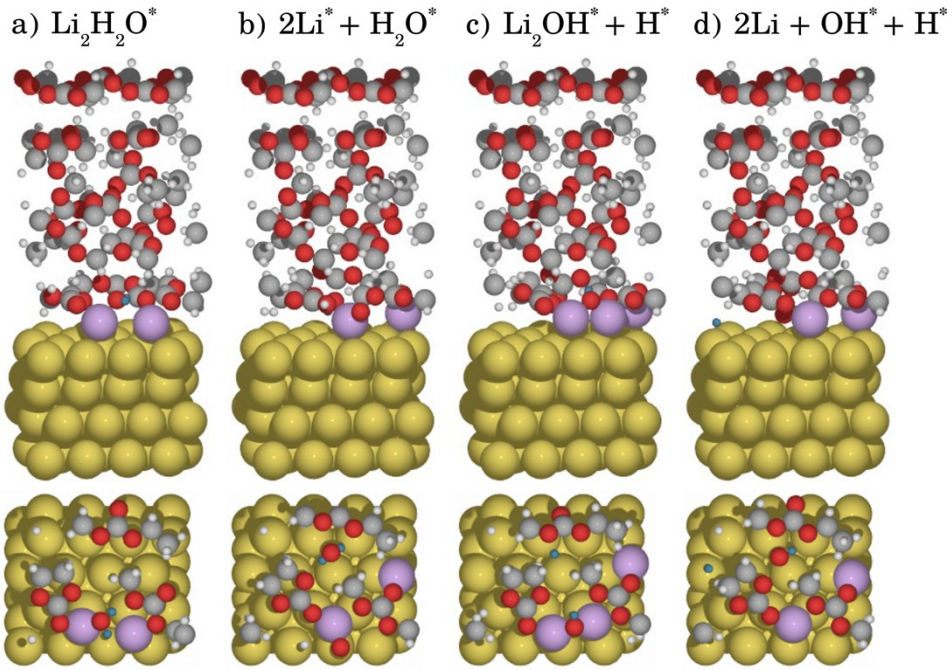

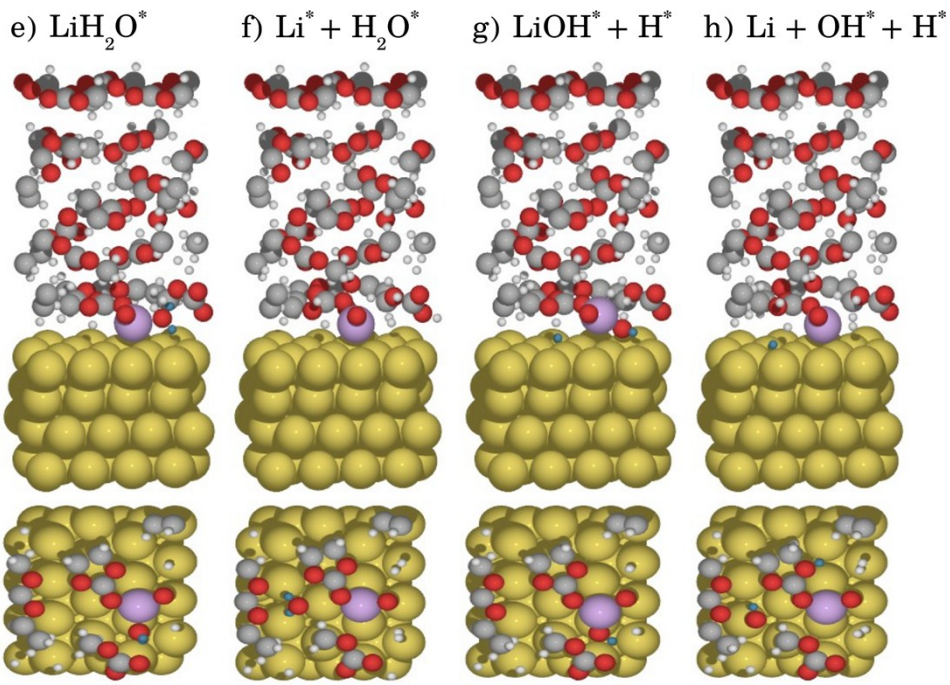

Figure S5: structures considered for the investigation of the LiO_x formation of Figure 2a.2.

Prediction of the limiting step for the LiF formation

As we have shown in Figure 2d and explained in the "Electrolyte simulations" section, we have identified two different limiting steps for the LiF formation. On Cu, Au, and Ir, in fact, the overpotential is determined by the presence of LiHF* at the interface, while for Pt, the adsorption of H* is the potential determining step. To understand this, we plot the correlation between the work function and the adsorption energy of H* (Figure S6). These two quantities are descriptors for the two relevant potential determining steps. In Figure S3, it is shown that the adsorption of LiF* is independent from the work function and the metal surface, and thus the only relevant quantity for the LiF*+H* level is the adsorption of H*. For LiHF*, instead, since it is computationally expensive to calculate the adsorption energy of LiHF* with the correct electrolyte structure, the work function can be used as a descriptor of the adsorption of LiHF*. Figure S6 shows that if the energy levels of LiHF* and LiF*+H* are aligned (either by changing the work function or the adsorption of H*), as indicated by the horizontal and vertical arrows, respectively, Au, Pt, and Ir lay on a line. The reason why Cu is off this line could be related with the electronic structure of the surface that make H* weakly adsorbed. This frontier can be used to predict which potential determining step is the relevant one for the design of novel anode materials.

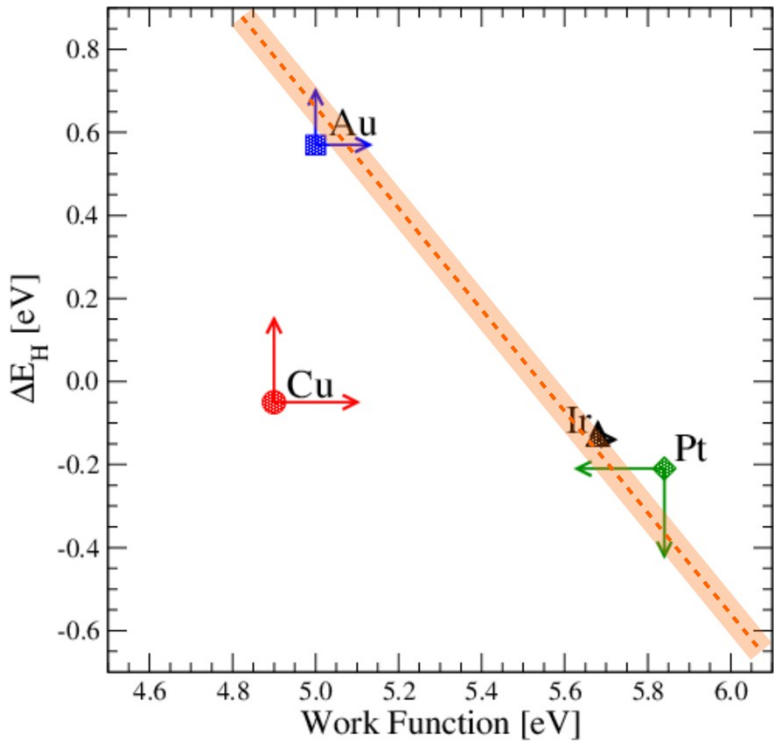

Figure S6: Correlation between the work function and the adsorption energy of H* for the 4 surfaces considered. The arrows indicates the shift in work function or adsorption energy that is required to align the energy levels of LiHF* and LiF*+H* of Figure 1.d. The frontier between the two possible potential determining steps is indicated in orange.

Different cations

CV experiments and the AIMD method has been applied to the situation when $NaPF_6$, instead of $LiPF_6$, is used as salt. The CVs are shown in Figure S7a and the DFT phase diagrams in Figure S7b. A small difference is seen between the potential of the electrochemical response corresponding to the H_2 evolution and formation of LiF and NaF, respectively, and this correlates with the simulations.

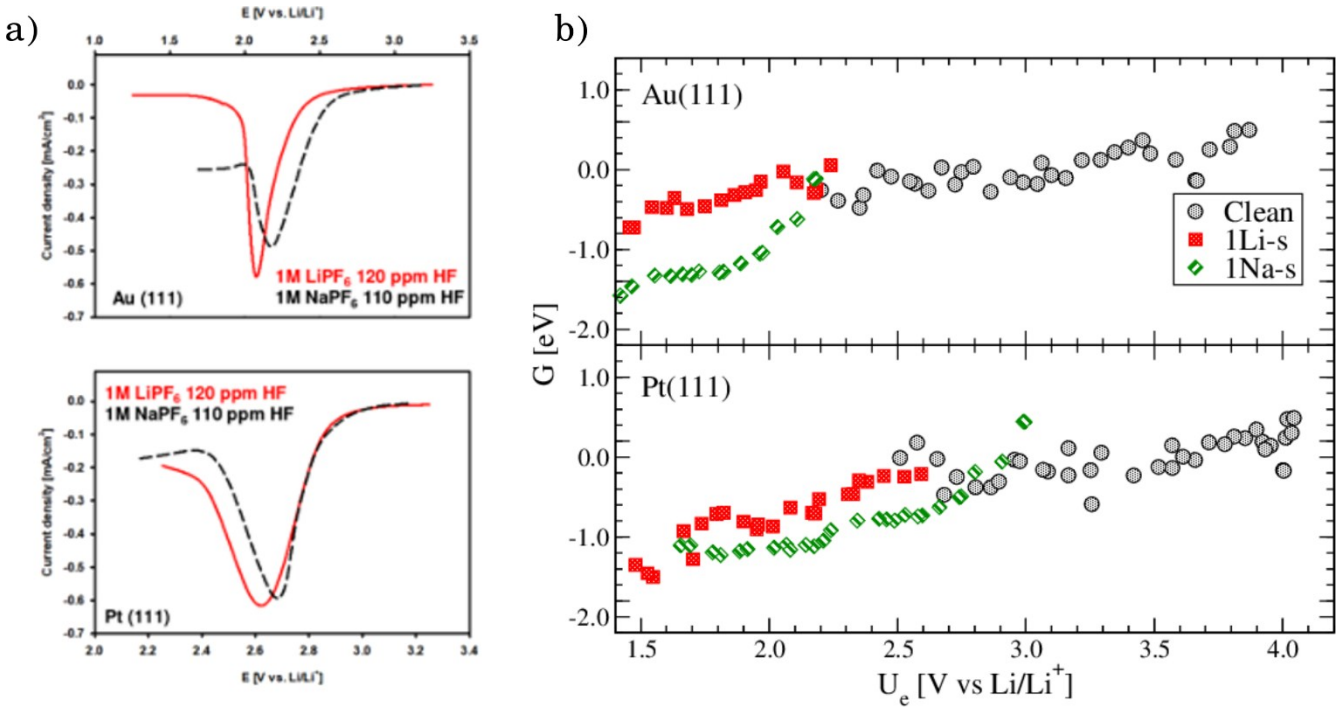

Figure S7: a) CVs of $LiPF_6$ and $NaPF_6$ on Au(111) and Pt(111), respectively. b) phase diagram of Li and Na in EC:EMC on Au(111) and Pt(111). The adsorption potential of the different cations shifts of less than 100 mV to a higher potential when Na is considered instead of Li. The potential scale for both calculations and experiments is Li/Li^+.

References:

1 J. J. Mortensen, L. B. Hansen and K. W. Jacobsen, Real-space grid implementation of the projector augmented wave method, *Phys. Rev. B*, 2005, **71**, 035109.

2 J. Enkovaara, C. Rostgaard, J. J. Mortensen, J. Chen, M. Dułak, L. Ferrighi, J. Gavnholt, C. Glinsvad, V. Haikola, H. A. Hansen, H. H. Kristoffersen, M. Kuisma, A. H. Larsen, L. Lehtovaara, M. Ljungberg, O. Lopez-Acevedo, P. G. Moses, J. Ojanen, T. Olsen, V. Petzold, N. A. Romero, J. Stausholm-Møller, M. Strange, G. A. Tritsaris, M. Vanin, M. Walter, B. Hammer, H. Häkkinen, G. K. H. Madsen, R. M. Nieminen, J. K. Nørskov, M. Puska, T. T. Rantala, J. Schiøtz, K. S. Thygesen and K. W. Jacobsen, Electronic structure calculations with GPAW: a real-space implementation of the projector augmented-wave method, *J. Phys. Condens. Matter*, 2010, **22**, 253202.

3 A. Hjorth Larsen, J. Jørgen Mortensen, J. Blomqvist, I. E. Castelli, R. Christensen, M. Dułak, J. Friis, M. N. Groves, B. Hammer, C. Hargus, E. D. Hermes, P. C. Jennings, P. Bjerre Jensen, J. Kermode, J. R. Kitchin, E. Leonhard Kolsbjerg, J. Kubal, K. Kaasbjerg, S. Lysgaard, J. Bergmann Maronsson, T. Maxson, T. Olsen, L. Pastewka, A. Peterson, C. Rostgaard, J. Schiøtz, O. Schütt, M. Strange, K. S. Thygesen, T. Vegge, L. Vilhelmsen, M. Walter, Z. Zeng and K. W. Jacobsen, The atomic simulation environment—a Python library for working with atoms, *J. Phys. Condens. Matter*, 2017, **29**, 273002.

4 J. Wellendorff, K. T. Lundgaard, A. Møgelhøj, V. Petzold, D. D. Landis, J. K. Nørskov, T. Bligaard and K. W. Jacobsen, Density functionals for surface science: Exchange-correlation model development with Bayesian error estimation, *Phys. Rev. B*, 2012, **85**, 235149.

5 M. H. Hansen and J. Rossmeisl, PH in Grand Canonical Statistics of an Electrochemical Interface, *J. Phys. Chem. C*, 2016, **120**, 29135–29143.

6 A. H. Larsen, M. Vanin, J. J. Mortensen, K. S. Thygesen and K. W. Jacobsen, Localized atomic

basis set in the projector augmented wave method, *Phys. Rev. B - Condens. Matter Mater. Phys.*, 2009, **80**, 1–10.
7 B. Hammer and L. Hansen, Improved adsorption energetics within density-functional theory using revised Perdew-Burke-Ernzerhof functionals, *Phys. Rev. B*, 1999, **59**, 7413–7421.
8 H. J. C. Berendsen, J. P. M. Postma, W. F. Van Gunsteren, A. Dinola and J. R. Haak, Molecular dynamics with coupling to an external bath, *J. Chem. Phys.*, 1984, **81**, 3684–3690.
9 C. W. Bunn, The crystal structure of ethylene, *Trans. Faraday Soc.*, 1944, **40**, 23.
10 C. J. Brown, The crystal structure of ethylene carbonate, *Acta Crystallogr.*, 1954, **7**, 92–96.
11 M. H. Hansen, A. Nilsson and J. Rossmeisl, Modelling pH and potential in dynamic structures of the water/Pt(111) interface on the atomic scale, *Phys. Chem. Chem. Phys.*, 2017, **19**, 23505–23514.
12 A. Bagger, L. Arnarson, M. H. Hansen, E. Spohr and J. Rossmeisl, Electrochemical CO Reduction: A Property of the Electrochemical Interface, *J. Am. Chem. Soc.*, 2019, **141**, 1506–1514.
13 D. Strmcnik, I. E. Castelli, J. G. Connell, D. Haering, M. Zorko, P. Martins, P. P. Lopes, B. Genorio, T. Østergaard, H. A. Gasteiger, F. Maglia, B. K. Antonopoulos, V. R. Stamenkovic, J. Rossmeisl and N. M. Markovic, Electrocatalytic transformation of HF impurity to H2 and LiF in lithium-ion batteries, *Nat. Catal.*, 2018, **1**, 255–262.